De novo variants in *ATP2B1* lead to neurodevelopmental delay

Authors

Meer Jacob Rahimi, Nicole Urban, Meret Wegler, ..., Richard Person, Rami Abou Jamra, Henry Oppermann

Correspondence

henry.oppermann@medizin.uni-leipzig.de

Rahimi et al., 2022, The American Journal of Human Genetics *109*, 944–952
May 5, 2022
https://doi.org/10.1016/j.ajhg.2022.03.009

CellPress

De novo variants in *ATP2B1* lead to neurodevelopmental delay

Meer Jacob Rahimi,[1] Nicole Urban,[2] Meret Wegler,[1] Heinrich Sticht,[3] Michael Schaefer,[2] Bernt Popp,[1] Frank Gaunitz,[4] Manuela Morleo,[5,6] Vincenzo Nigro,[5,6] Silvia Maitz,[7] Grazia M.S. Mancini,[8] Claudia Ruivenkamp,[9] Eun-Kyung Suk,[10] Tobias Bartolomaeus,[1,11] Andreas Merkenschlager,[12] Daniel Koboldt,[13] Dennis Bartholomew,[14] Alexander P.A. Stegmann,[15] Margje Sinnema,[15] Irma Duynisveld,[16] Ramona Salvarinova,[17] Simone Race,[17] Bert B.A. de Vries,[18] Aurélien Trimouille,[19,20] Sophie Naudion,[21] Daphna Marom,[22] Uri Hamiel,[22] Noa Henig,[22] Florence Demurger,[23] Nils Rahner,[24] Enrika Bartels,[24] J. Austin Hamm,[25] Abbey M. Putnam,[25] Richard Person,[26] Rami Abou Jamra,[1] and Henry Oppermann[1,*]

Summary

Calcium (Ca^{2+}) is a universal second messenger involved in synaptogenesis and cell survival; consequently, its regulation is important for neurons. ATPase plasma membrane Ca^{2+} transporting 1 (ATP2B1) belongs to the family of ATP-driven calmodulin-dependent Ca^{2+} pumps that participate in the regulation of intracellular free Ca^{2+}. Here, we clinically describe a cohort of 12 unrelated individuals with variants in *ATP2B1* and an overlapping phenotype of mild to moderate global development delay. Additional common symptoms include autism, seizures, and distal limb abnormalities. Nine probands harbor missense variants, seven of which were in specific functional domains, and three individuals have nonsense variants. 3D structural protein modeling suggested that the variants have a destabilizing effect on the protein. We performed Ca^{2+} imaging after introducing all nine missense variants in transfected HEK293 cells and showed that all variants lead to a significant decrease in Ca^{2+} export capacity compared with the wild-type construct, thus proving their pathogenicity. Furthermore, we observed for the same variant set an incorrect intracellular localization of ATP2B1. The genetic findings and the overlapping phenotype of the probands as well as the functional analyses imply that *de novo* variants in *ATP2B1* lead to a monogenic form of neurodevelopmental disorder.

Global developmental delay (DD), often leading to intellectual disability (ID), has a high prevalence of about 2% and is among the most frequent indications for genetic testing.[1] Despite its frequency and importance, a genetic cause can only be found in 27% to 42% of routine diagnostic cases.[2,3] One reason for this inadequate clarification rate is the extreme genetic heterogeneity of DD. According to the SysNDD[4] database, pathogenic variants in 1,497 (gene statistics from July 29, 2021) different genes are an established cause of a neurodevelopmental disorder. Furthermore, several genes are under investigation to identify their association with DD/ID.

Calcium (Ca^{2+}) is a second messenger that is involved in the regulation of signal transduction, gene expression, cell metabolism, and cell survival. Ca^{2+} homeostasis is especially important for neurons, as it controls the release of neurotransmitters and regulates neurite outgrowth, cell membrane depolarization, and depression of synaptic transmission, which are important processes for learning and memory consolidation (for a review, see Brini et al.[5]). The dysregulation of Ca^{2+} homeostasis by pathogenic variants in Ca^{2+} channel genes, such as *CACNA1A* (MIM: 183086), is a common cause for several forms of ataxia. Moreover, other genes whose protein products control

[1]Institute of Human Genetics, University of Leipzig Hospitals and Clinics, Leipzig 04103, Germany; [2]Rudolf-Boehm-Institute of Pharmacology and Toxicology, University of Leipzig Hospitals and Clinics, Leipzig 04107, Germany; [3]Institute of Biochemistry, Friedrich-Alexander-Universität Erlangen-Nürnberg, Erlangen 91054, Germany; [4]Department of Neurosurgery, University of Leipzig Hospitals and Clinics, Leipzig 04103, Germany; [5]Telethon Institute of Genetics and Medicine, Pozzuoli, 80078 Naples, Italy; [6]Department of Precision Medicine, University of Campania "Luigi Vanvitelli," Naples 80138, Italy; [7]Clinical Pediatric Genetic Unit, Pediatric Clinic, Fondazione MBBM, San Gerardo Hospital, Monza 20900, Italy; [8]ErasmusMC University Medical Center, Department of Clinical Genetics, Rotterdam 3015, the Netherlands; [9]Leiden University Medical Center, Clinical Genetics, Leiden 2333, the Netherlands; [10]Praxis für Humangenetik-Friedrichstrasse, Berlin 10117, Germany; [11]CeGaT GmbH and Praxis für Humangenetik Tübingen, Tübingen 72076, Germany; [12]Department of Neuropediatrics, University of Leipzig Hospitals and Clinics, Leipzig 04103, Germany; [13]Institute for Genomic Medicine at Nationwide Children's Hospital, Columbus, OH 43205, USA; [14]Division of Genetic and Genomic Medicine at Nationwide Children's Hospital, Columbus, OH 43205, USA; [15]Department of Clinical Genetics, Maastricht University Medical Center+, Maastricht 6229, the Netherlands; [16]Severinus Institute for Intellectual Disability, 5507 Veldhoven, the Netherlands; [17]Division of Biochemical Genetics, Department of Pediatrics, University of British Columbia, BC Children's Hospital, Vancouver, BC V6H 3N1, Canada; [18]Department of Human Genetics, Donders Institute for Brain, Cognition and Behaviour, Radboud University Medical Center, Nijmegen 6525, the Netherlands; [19]Service de Pathologie Centre Hospitalier Universitaire de Bordeaux, Bordeaux 33000, France; [20]MRGM, Maladies Rares: Génétique et Métabolisme, INSERM U1211, Université de Bordeaux, Bordeaux 33076, France; [21]Service de Génétique Médicale, Centre Hospitalier Universitaire de Bordeaux, Bordeaux 33076, France; [22]The Genetics Institute, Tel Aviv Sourasky Medical Center and Sackler Faculty of Medicine, Tel Aviv University, Tel Aviv 6423906, Israel; [23]Service de Génértique, CHBA, Vannes 56000, France; [24]Institute for Clinical Genetics, Bonn 53111, Germany; [25]Pediatric Genetics, East Tennessee Children's Hospital, Knoxville, TN 37916, USA; [26]Clinical Genomics Program, GeneDx, Inc., Gaithersburg, MD 20877, USA

*Correspondence: henry.oppermann@medizin.uni-leipzig.de

https://doi.org/10.1016/j.ajhg.2022.03.009.

Table 1. Clinical spectrum of the *ATP2B1*-related disorder

Individual	Variant	Inheritance	Sex	Age[a]	DD	ID	Behavior	Seizures	Other
1	c.716A>G (p.Asp239Gly)	*de novo*	F	6 years	yes	moderate	normal	yes	secundum atrial septal defect, toe clindactyly, facial dysmorphism, hypotonia
2	c.791C>T (p.Thr264Ile)	*de novo*	M	8 years	yes	mild	ASD	no	transposition of large vessels, low set ears
3	c.1274C>A (p.Thr425Lys)	*de novo*	M	9 years	yes	mild	N/A	pathological EEG	cerebral cavernous malformation, sparse hair
4	c.1376A>G (p.His459Arg)	*de novo*	M	17 years	yes	mild	ASD	yes	marfanoid habitus, arachnodactyly, scoliosis, hypermobile thumb
5	c.2288G>C (p.Arg763Pro)	*de novo*	M	21 years	yes	mild	ASD	no	facial dysmorphism
6	c.2365C>T (p.Arg789Cys)	*de novo*	M	3 years	yes	unclassified	sleeping difficulties	yes	facial dysmorphism, hypotonia
7	c.2470G>A (p.Glu824Lys)	*de novo*	F	22 years	yes	moderate	compulsive behavior	yes	N/A
8	c.2570A>G (p.Gln857Arg)	*de novo*	F	3 years	yes	unclassified	normal	no	brachycephaly, facial dysmorphism, clinodactyly of the 5th finger
9	c.2972G>A (p.Arg991Gln)	unknown	M	51 years	yes	mild	ASD	no	marfanoid habitus, aortic root dilation, pectus carinatum, scoliosis, arachnodactyly, facial dysmorphism
10	c.2632C>T (p.Gln878*)	*de novo*	M	6 years	yes	mild	hyperactivity	no	facial dysmorphism
11	c.458G>A (p.Trp153*)	unknown	F	6 years	yes	moderate	N/A	no	short stature
12	c.1789C>T (p.Arg597*)	unknown	M	5 years	yes	unclassified	ASD	infantile spasms	short stature, pectus excavatum, plagiocephaly

Abbreviations: ID, intellectual disability; DD, development delay; ASD, autism spectrum disorder; N/A, not available; M, male; F, female. Variant descriptions based on GenBank: NM_001001323.2.
[a]Age of last examination.

intracellular levels of free Ca^{2+}, such as *CACNA1B* (MIM: 618497),[6] *CAMK4*,[7] *ANXA11*,[8] and *MICU2*,[9] have been reported to be associated with DD/ID.

ATPase plasma membrane Ca^{2+} transporting 1 (*ATP2B1*, formerly known as plasma membrane Ca^{2+} pump isoform 1; *PMCA1*; MIM: 108731) encodes an ATP-driven calmodulin-dependent Ca^{2+} pump that maintains the homeostasis of intracellular Ca^{2+} by removing it from the cytosol. Moreover, Ca^{2+} pumps are considered to have a crucial role on neuronal function (for a review, see Calì et al.[10]) and certain variants in isoforms of *ATP2B1* have been reported to be pathogenic. Cali and colleagues[11] reported one individual with DD, generalized hypotonia, cerebellar ataxia, and a hemizygote missense variant in *ATP2B3* (MIM: 302500). In another case report, Li and colleagues[12] describe four members of Chinese family with progressive spastic paraplegia and a heterozygous missense variant in *ATP2B4*.

In this study, we report 12 individuals with an overlapping phenotype of mild to moderate DD/ID, each harboring a different variant in *ATP2B1*. Table 1 presents an outline of the clinical symptoms of each individual. Additionally, a comprehensive clinical description of each individual is in Table S1 and in the supplemental

Figure 1. Photos of individuals with *ATP2B1* variants
No shared dysmorphic features in four individuals (for individual numbering, see Table 1).

notes. Written consents for genetic testing and its publication, as well as the publication of photographs, were obtained from all subjects studied or their legal representatives after counseling and information about risks and benefits in accordance with national ethical standards and laws as confirmed by the responsible local committees. This study was approved by the ethics committee of the University of Leipzig (approval code: 402/16-ek).

All individuals showed clear signs of DD. These included speech development delay in all individuals with a median age of first words of 26 months (spectrum of 12 to 36 months) and motor development delay in most individuals (median age at first walking 20 months; 16 to 36 months). The DD/ID was of variable degree; borderline to mild: 7/12, 58%; moderate: 3/12, 25%; moderate to severe: 2/12, 17%. Furthermore, five individuals (5/11, 45%, no information on one proband) were diagnosed with an autism spectrum disorder (ASD) and three additional individuals showed other behavior abnormalities. Dissimilar forms of seizures were reported in six individuals (6/12, 50%). Noteworthy, abnormal brain MRI findings were reported in three individuals without overlapping aspects. Individuals 1 and 6 had hypotonia. Other neurological symptoms, such as ataxia, were not reported. Individuals 11 and 12 had short stature, while all other individuals had normal growth development. Of note, two individuals, 4 and 9, exhibited a marfanoid habitus. Although minor facial dysmorphisms have been reported by six individuals (individuals 1, 5, 6, 8, 9, and 10), there was no apparent shared facial gestalt nor specific malformations (Figure 1, Table S1). Additionally, four individuals had anomalies of digits (individuals 1, 4, 8, and 9).

According to data from gnomAD,[13] *ATP2B1* contains a significantly reduced number of truncating and missense variants, indicating a selective constraint on both types of variants in a population without severe, early-onset phenotypes such as DD/ID (probability of being loss-of-function intolerant [pLI] score = 1.00; *Z* score missense = 5.29). In the present cohort, we identified 12 variants in *ATP2B1*, nine missense and three nonsense, that we consider of relevance. Nine (eight missense and one nonsense) were detected *de novo*, while for the remaining three individuals, parents were unavailable for segregation. All variants were absent from gnomAD, except the *de novo* variant from individual 6 (c.2365C>T [p.Arg789Cys]), which was detected in gnomAD once. The three truncating variants affect neither the last exon, the last 55 bp of the penultimate exon, nor the first 100 bp of *ATP2B1*; thus, nonsense-mediated mRNA decay is likely.[14] The missense variants seem to be pathogenic *in silico* (conserved and predicted pathogenic by multiple tools) and have a combined annotation-dependent depletion (CADD)[15] score between 25.6 and 32 (mean 28.5) and a rare exome variant ensemble learner (REVEL)[16] score between 0.85 and 0.98 (mean 0.92, overview in Table S1). Additionally, seven out of nine missense variants of the cohort are located in established domains of ATP2B1 (Figure 2), which are critical for the protein's function. The E1-E2 ATPase as well as the cation transporter ATPase domains, which are affected by six variants, are involved in Ca^{2+} binding, phosphoenzyme formation, and Ca^{2+} release.[17] The haloacid dehalogenase-like hydrolase domain is affected by two variants and generates the energy for Ca^{2+} transport via hydrolysis of ATP to ADP. Two missense variants do not affect an established domain but are located in areas that are intolerant to missense variation, as proposed by MetaDome.[18] Hence, an altered protein function of these seems plausible.

To better understand how missense variants affect ATP2B1 function, we investigated the effect of the variants

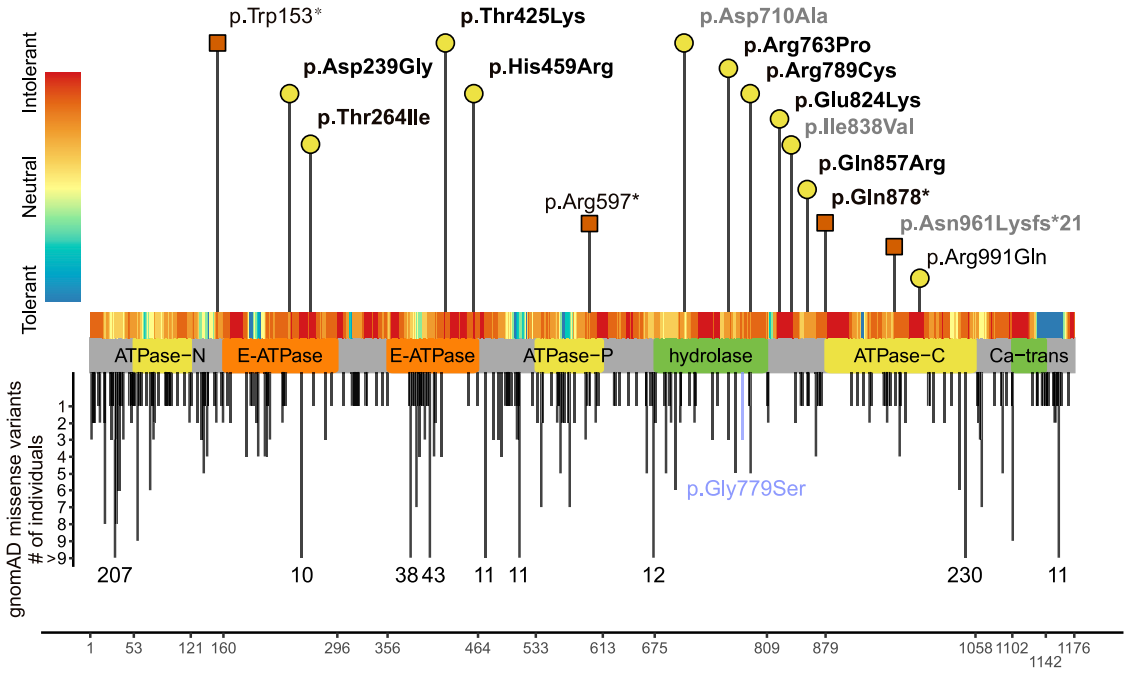

Figure 2. Variants in *ATP2B1*

Location of missense and loss-of-function variant in *ATP2B1* with respect to the domain structure of ATP2B1 (GenBank: NM_001001323.2). The x axis represents the corresponding amino acid position of ATP2B1. Variants reported in this study are labeled with the corresponding p-code and are indicated by a yellow circle (missense) or a red square (loss of function). Confirmed *de novo* variants are indicated in bold. Deciphering Developmental Disorders study variants with a lacking detailed phenotypic description are indicated in gray (see also Table S1 and supplemental methods). Missense variants in gnomAD with allele count are shown below the protein scheme. The gnomAD variant p.Gly779Ser, which was used as negative control for the Ca^{2+} imaging experiments, is blue color-coded. The tolerance landscape (MetaDome[18]) is shown color-coded above the protein scheme. Abbreviations: ATPase-N, cation transporter/ATPase, N terminus; ATPase-P, cation transport ATPase (P-type); ATPase-C, cation transporter/ATPase, C terminus; E-ATPase, E1-E2 ATPase; hydrolase, haloacid dehalogenase-like hydrolase; Ca-trans, plasma membrane calcium transporter ATPase C-terminal.

by an *in silico* structural protein modeling. The availability of an experimental structure for ATP2B1[19] allows us to map the sequence positions of the variants in the 3D structure (Figure 3A). Three missense variants affect conserved amino acid (AA) residues in the transmembrane domain (Thr425, Gln857, and Arg991) that constitutes the Ca^{2+} exit pathway to the extracellular space. The remaining variants affect AA residues in the cytosolic protein part that harbors the active site. The observation that damaging variants are distributed over the structure is in line with the fact that ATP2B1 is a complex molecular machine that requires structural integrity of all domains for proper function.

Most of the residues affected by the identified variants form tight interactions in the protein structure and are predicted to affect protein stability by a variety of structural mechanisms: for example, p.Thr264Ile results in a loss of a stabilizing hydrogen bond (Figures 3B and 3C). The p.Gln857Arg exchange causes protein destabilization by a steric clash between the Arg857 and Met928 sidechain in the altered protein (Figures 3D and 3E). The p.Arg991Gln exchange most likely causes the loss of a stabilizing interaction between the positively charged arginine and the negatively charged phospholipids. The p.Thr425Lys exchange in the transmembrane domain generates a positive charge close to the Ca^{2+} exit pathway, which most likely interferes with the transport of the positively charged Ca^{2+} ions. The p.Asp710Ala exchange disrupts a salt-bridge between the Asp710 sidechain and a conserved lysine (Lys476) of the active site.

As the *in silico* predictions suggest that the variants would affect the function of ATP2B1, we tested this assumption experimentally. Therefore, we generated plasmids expressing *ATP2B1* that harbor the variants of interest. Although the variants in our cohort affect several isoforms of ATP2B1, we decided to investigate the isoform (ATP2B1a) that is mainly detected in the human brain[20] (GenBank: NM_001001323.2; Ensembl: ENST00000359142.7; compare also GTEx for expression data). As expected, we observed a membranous fluorescence after transfection of the ATP2B1-yellow fluorescent protein (YFP) wild-type expression plasmid in HEK293 cells (Figure 4A). More important, we also observed a significantly altered cellular localization of ATP2B1-YFP harboring the variants p.Asp239Gly, p.Thr264Ile, and p.Arg991Gln (Figures 4A and 4B). Of the remaining six missense variants, the variants p.Thr425Lys, p.Arg763Pro, p.Glu824Lys, and p.Gln857Arg also showed a shift of membranous to cytoplasmatic localization of ATP2B1. However, this effect was not statistically significant, as

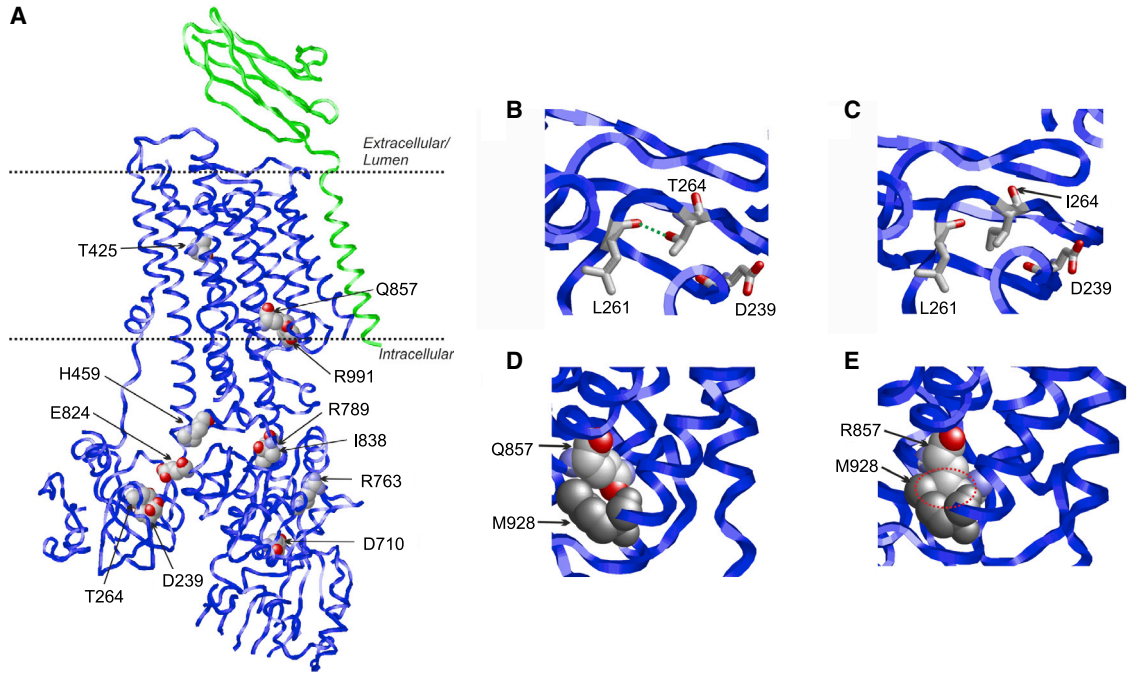

Figure 3. Structural effects in ATP21B1
(A) Structure of ATP2B1 (PDB: 6A69[19]) indicating the sites of genetic variants. The ATP2B1 structure is shown as blue ribbon and the neuroplastin subunit in green. Sites of genetic variants are shown in space-filled presentation (atom-type coloring) and labeled. The location of the membrane is indicated by two dotted lines.
(B) Enlargement of the ATP2B1 structure showing the effect of the p.T264Ile and p.Gln857Arg variants. (B) T264 forms a hydrogen bond (green dotted line) to L261.
(C) In the p.Thr264Ile variant, this hydrogen bond cannot be formed by the nonpolar isoleucine sidechain.
(D) Q857 is in close spatial proximity to M928 (shown in gray).
(E) The bulkier R857 sidechain of the variant causes steric clashes (red dotted circle) with M928 leading to a destabilization of ATP2B1.

this was observable only in a proportion of analyzed cells (Figure S1). The variants p.His459Arg and p.Arg789Cys did not show a change and were comparable with the wild type.

Next, we investigated whether the identified variants in *ATP2B1* affect the Ca^{2+} transport function of ATP2B1. Therefore, we performed $[Ca^{2+}]_i$ imaging in HEK293 cells after transfection of the corresponding expression plasmids. We chose this method[21] because it allows a continuous measurement with a perfusion system to infuse the cells with different solutions. This makes it possible for us to investigate the cells in an approximate physiological environment and change of cellular Ca^{2+} gradients. The method allows even higher sensitivity because transfected cells can be separated from non-transfected ones by single-handedly picking the cells with a YFP signal, expressed through the plasmid. The result of this experiment is shown in Figure 5A. To investigate the ATP2B1 activity, we determined the relative Ca^{2+} extrusion rate. Therefore, after initial perfusion with EGTA, Ca^{2+} store depletion, and Ca^{2+} loading, we analyzed $[Ca^{2+}]_i$ decline after perfusion with EGTA, which is represented by the time constant tau (see also Figure S2). Hence, a lower tau value indicates a higher ATP2B1 activity. Accordingly, we could detect a significantly reduced tau value after transfection of the wild-type ATP2B1 plasmid compared to untransfected HEK293 cells (Figure 5B). As an additional negative control, we analyzed a presumably non-pathogenic variant (p.Gly779Ser) that was detected three times in gnomAD. As expected, the $[Ca^{2+}]_i$ imaging experiments revealed no statistically different Ca^{2+} extrusion rate of this variant compared to the wild type. The investigation of the identified variants in the present cohort revealed a significantly increased tau value after Ca^{2+} loading in all nine variants compared to the wild type (Figure 5B).

Interestingly, by ranking the variants on the basis of reduction of Ca^{2+} transport and on changes in cellular localization, we observe a significant correlation between the influence of a *ATP2B1* variant on membrane localization and the tau value ($p < 0.001$; $r^2 = 0.768$; Figure S3A). Of note, we also found a correlation between the REVEL score and the tau value ($p < 0.02$; $r^2 = 0.5$; Figure S3B) on the basis of the rank. Although speculative, these observations indicate that the missense variants identified in this study reduce Ca^{2+} transport by disturbing the cellular trafficking and/or by inducing the degradation of abnormal ATP2B1 protein. A similar mechanism has also been reported for the creatine transporter *SLC6A8*.[22]

At this point, it should be noted that we identified another individual with DD and a *de novo* variant in *ATP2B1* (c.1793T>C [p.Ile598Thr]; see supplemental note, "individual 16"). We have not included this

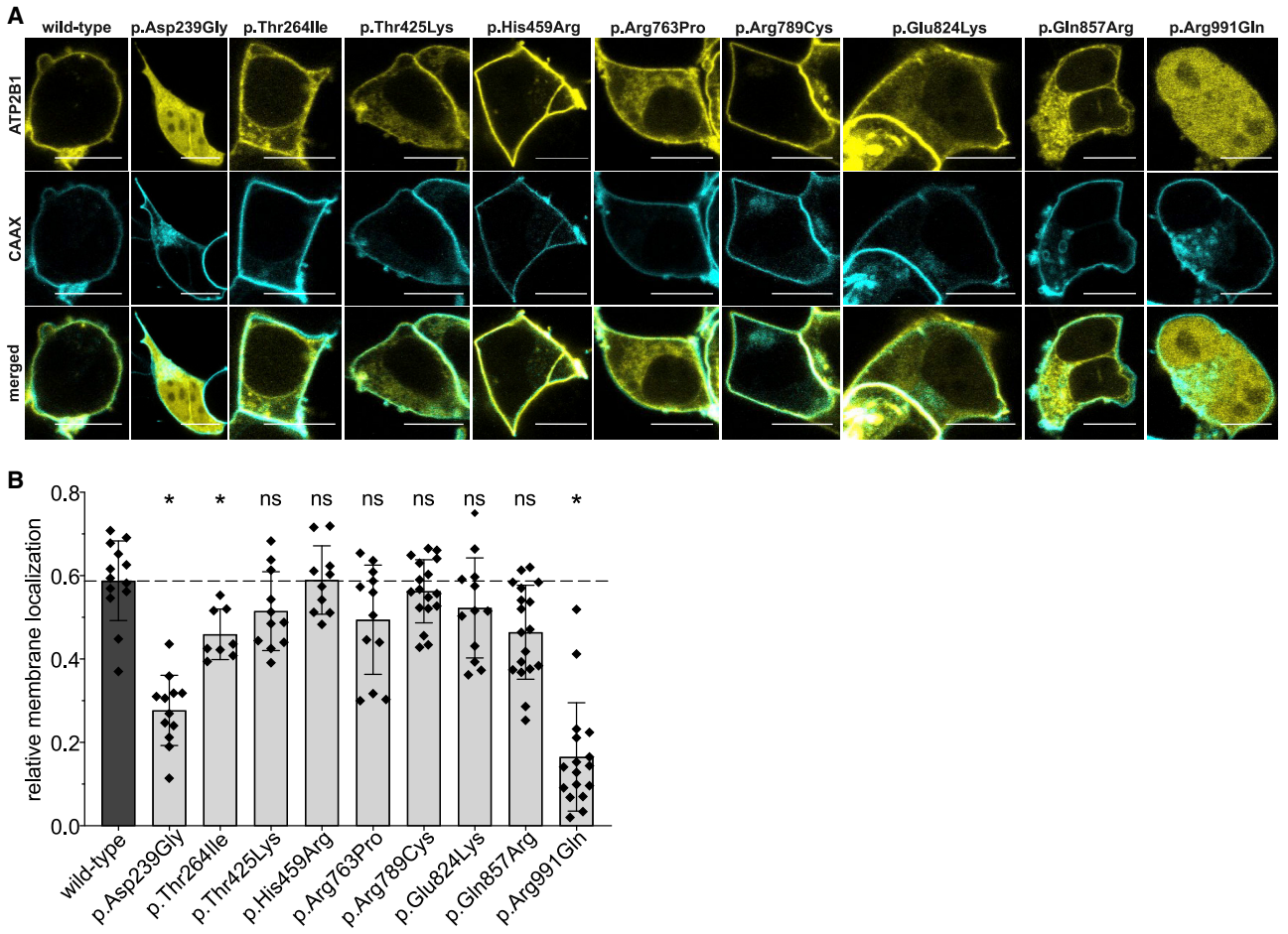

Figure 4. Subcellular localization of transiently overexpressed *ATP2B1* variants

(A) Representative confocal laser scanning microscopy images of transfected HEK293 cells expressing YFP-fused ATP2B1 and a CAAX-box-modified cyan fluorescent protein. Scale bars: 10 μm.

(B) Quantification of relative membrane localization (for details, see supplemental methods). Data presented as mean and standard deviation from 8 to 17 independent analyzed cells. Data are shown as mean ± standard deviation represented by error bars. The results of a one-way ANOVA with the Games-Howell post-hoc test (each compared to wild type) is indicated as: *$p < 0.05$; ns: $p > 0.05$.

individual into the clinical description of the present cohort, as the membrane localization and the tau value were indistinguishable from the wild type. It is possible that the variant causes a functional effect not measured by our assays. However, because the clinical relevance of this variant remains uncertain, we have excluded this individual from the phenotypic analysis.

The results of the present study imply that *de novo* missense variants in *ATP2B1* cause a loss-of-function mechanism on the basis of the following observations. (1) The *in silico* structural modeling supports a reduced ATP2B1 activity resulting from changes of protein structure or stability. (2) The Ca^{2+} transport is significantly decreased by the missense variants. (3) The correlation between intracellular localization and tau value suggests the degradation of abnormal ATP2B1. (4) *ATP2B1* exhibits a pLI score = 1.00, which supports a potential haploinsufficiency of this gene. (5) Three of the probands carry nonsense variants. This notion is further supported by the reports of seven independent individuals that harbor gross deletions, which affect *ATP2B1* (summarized by Klein et al.[23] and James et al.[24]). More important, these individuals exhibited an overlapping phenotype (DD, digit anomalies, facial dysmorphism, and growth deficiency) with the probands reported in the present study. We cannot exclude a dominant negative effect by the missense variants, even though this mechanism is unlikely. Instead of acting as monomers or homodimers, ATP2B1–4 form heteromeric complexes with neuroplastin or basigin.[25] In accordance, none of the missense variants affect the interacting region of ATP2B1 and neuroplastin (Figure 3A).

Taken together, the overlapping phenotype of the probands and the experimental evidence strongly support that *ATP2B1* is a DD/ID-associated gene. Furthermore, the role of *ATP2B1* in neurodevelopment is strengthened by its expression pattern. While *ATP2B1* is expressed at the early stages during development, the three other isoforms of the ATPase plasma membrane Ca^{2+} transporter family (*ATP2B2–4*) are expressed at later stages.[26] The

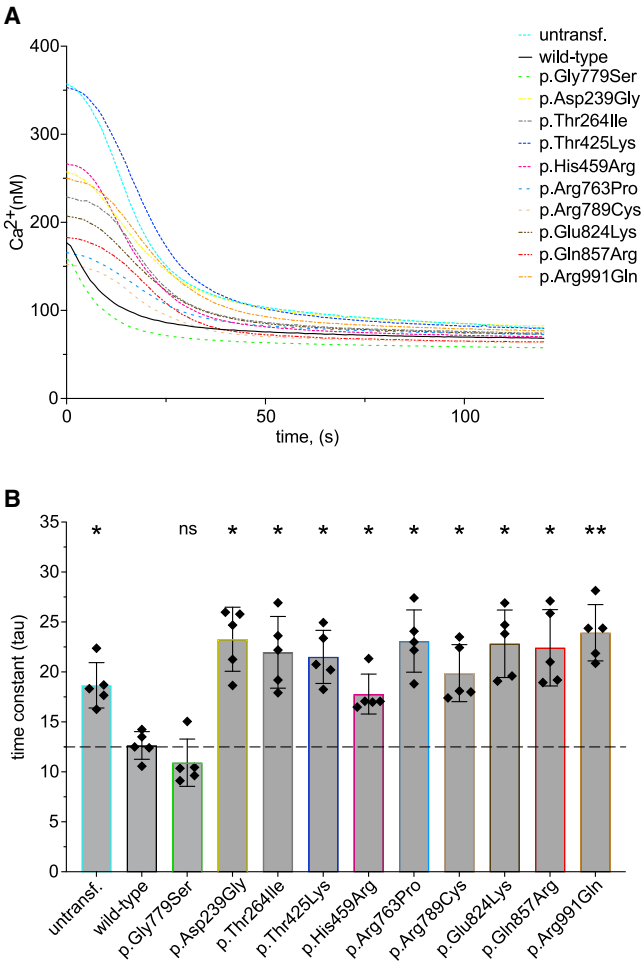

Figure 5. *De novo* missense variants in *ATP2B1* affect Ca^{2+} transport

(A) Fluorometric $[Ca^{2+}]_i$ analysis (for details, see supplemental methods) in untransfected (untransf.) HEK293 cells and cells expressing wild-type or mutated ATP2B1. Data are shown as mean $[Ca^{2+}]_i$ from five independent experiments after loading of the $[Ca^{2+}]_i$ indicator dye fura-2/AM and the final addition of EGTA (for a representative complete sequence of the experiment, see Figure S2).

(B) In order to investigate the Ca^{2+} transport of transfected HEK293, time-dependent $[Ca^{2+}]_i$ decline was analyzed after final addition of EGTA that is represented by the time constant tau. Data presented as mean and standard deviation from five independent experiments. As negative control served the likely non-pathogenic variant (3 times in gnomAD) p.Gly779Ser. The dashed line indicates the median tau value of ATP2B1 wild type. Data are shown as mean ± standard deviation represented by error bars. The results of a one-way ANOVA with the Games-Howell post-hoc test (each compared to wild type) is indicated as: ** $p < 0.005$; *$p < 0.05$; ns: $p > 0.05$.

important role of *ATP2B1* for neurological development is further corroborated by the fact that it can compensate for the absence of those other isoforms to a certain extent.[27] *ATP2B1* encodes different isoforms, which differ in calmodulin affinity and tissue expression, by alternative splicing (for a review, see Krebs[28]). Kenyon and colleagues found that Atp2b1b is nearly ubiquitously expressed in most tissues, while Aatp2ba is specifically expressed in the central nervous system. In rat brains, they found out that Atp2b1a is detected only in neurons, where it concentrates in the membrane of the soma, dendrites, and spines.[20] It thus seems logical to consider *ATP2B1* as a candidate gene for an early neurodevelopmental disorder as diagnosed in the probands of this study. Atp2b1–4 accumulate during the maturation of hippocampal neurons, which indicates the need of an increased Ca^{2+}-exclusion capacity.[26] Interestingly, Atp2b1–4 are transcriptionally regulated by Ca^{2+} itself.[29] Likewise, studies with rats demonstrated the expression of ATP2B1b in the developing brain is later replaced by ATP2B1a, therefore further underlining its role in neurodevelopment.[30]

Thus, as *ATP2B1* has a significant impact on Ca^{2+} homeostasis in the central nervous system[31] during development on the basis of its expression pattern, it strongly supports that variants that affect ATP2B1's function will impact neurons and therefore an individual's neurodevelopment.

We also considered whether variants that affect a certain domain lead to a variable phenotype. However, we could observe neither a particular domain-specific correlation with the symptoms of the individuals nor a correlation between the severity of the symptoms and the impact of each variant on ATP2B1 activity. This may be due to the relatively small size of the herein reported cohort. Therefore, further studies with more individuals harboring a pathogenic variant in *ATP2B1* may clarify a potential correlation.

In conclusion, the overlapping phenotype of 12 probands, the genetic findings, the *in silico* data, the structural modeling, the role of *ATP2B1* in the central nervous system, and the pathogenicity of the variants prompt us to add *ATP2B1* loss-of-function variants as a monogenetic cause of DD/ID.

Data and code availability

The data of this study are available from the corresponding author with reasonable request. There was no code used for this study.

Supplemental information

Supplemental information can be found online at https://doi.org/10.1016/j.ajhg.2022.03.009.

Author contributions

M.J.R., R.J., M.W., and H.O. contributed to the concept and design and coordinated the study. Data curation and genetic analysis were performed by D.K., D.M., N.H., A.T., M.M., V.N., R.P., A.S., and T.B. Clinical investigations were performed by G.M., D.B., S.M., F.M., B.V., D.M., U.H., S.N., N.R., E.B., M. Sinnema, A.M., and I.D. The experiments were performed by M.J.R., N.U., and H.O. under the support of F.G. and M. Schaefer. H.S. performed the structural analysis and molecular modeling. M.J.R. and H.O. contributed to the acquisition, interpretation, statistical analysis, and visualization of the results. The original draft was written by M.J.R., R.J., and H.O., and all authors critically revised the

manuscript and ensured the final approval of the manuscript for publication.

Acknowledgments

The authors would like to thank the proband's families for their support and consent to the study. M.M. and V.N. were supported by the Telethon Undiagnosed Diseases Program (TUDP, GSP15001). The experiments were funded by budget resources of the Institute of Human Genetics (Leipzig, Germany), the Department of Neurosurgery (Leipzig, Germany), the Rudolf-Boehm-Institute of Pharmacology and Toxicology (Leipzig, Germany), and the Institute of Biochemistry (Erlangen, Germany). This work was generated within ITHACA: European Reference Network on Rare Congenital Malformations and Rare Intellectual Disability (M. Sinnema). We would also like to thank Patrick Yap and Polona Le Quesne Stabej from the University of Auckland, New Zealand for the fruitful discussions. Last but not least, we would like to thank the reviewers for the constructive comments that significantly improved the present work.

Declaration of interests

R.P. is an employee of GeneDx, Inc. All other authors declare no competing interests.

Received: October 14, 2021
Accepted: March 11, 2022
Published: March 30, 2022

Web resources

DECIPHER, https://www.deciphergenomics.org/
ENSEMBL, https://www.ensembl.org/
GeneMatcher, https://genematcher.org/
GenBank, https://www.ncbi.nlm.nih.gov/genbank/
gnomAD, https://gnomAD.broadinstitute.org/
MetaDome, https://stuart.radboudumc.nl/metadome
MutationTaster, https://www.mutationtaster.org/
OMIM, http://www.omim.org/
STRING database, https://www.string-db.org/
SysNDD, https://www.sysid.dbmr.unibe.ch/
The Genotype-Tissue Expression (GTEx) Project, https://gtexportal.org/home/
The National Center for Biotechnology Information (NCBI), https://www.ncbi.nlm.nih.gov/
UCSC Cell Browser (human cerebral cortex), http://hgw1.soe.ucsc.edu/
UniProt database, https://www.uniprot.org/
Variant Effect Predictor (VEP) from ENSEMBL, https://www.ensembl.org/Tools/VEP
WebAutoCasC, https://autocasc.uni-leipzig.de/

References

1. McRae, J.F., Clayton, S., Fitzgerald, T.W., Kaplanis, J., Prigmore, E., Rajan, D., Sifrim, A., Aitken, S., Akawi, N., Alvi, M., et al. (2017). Prevalence and architecture of de novo mutations in developmental disorders. Nature *542*, 433–438.
2. Gilissen, C., Hehir-Kwa, J.Y., Thung, D.T., van de Vorst, M., van Bon, B.W., Willemsen, M.H., Kwint, M., Janssen, I.M., Hoischen, A., Schenck, A., et al. (2014). Genome sequencing identifies major causes of severe intellectual disability. Nature *511*, 344–347.
3. Aspromonte, M.C., Bellini, M., Gasparini, A., Carraro, M., Bettella, E., Polli, R., Cesca, F., Bigoni, S., Boni, S., Carlet, O., et al. (2019). Characterization of intellectual disability and autism comorbidity through gene panel sequencing. Hum. Mutat. *40*, 1346–1363.
4. Kochinke, K., Zweier, C., Nijhof, B., Fenckova, M., Cizek, P., Honti, F., Keerthikumar, S., Oortveld, M.A.W., Kleefstra, T., Kramer, J.M., et al. (2016). Systematic Phenomics Analysis Deconvolutes Genes Mutated in Intellectual Disability into Biologically Coherent Modules. Am. J. Hum. Genet. *98*, 149–164.
5. Brini, M., Calì, T., Ottolini, D., and Carafoli, E. (2014). Neuronal calcium signaling: function and dysfunction. Cell. Mol. Life Sci. *71*, 2787–2814.
6. Gorman, K.M., Meyer, E., Grozeva, D., Spinelli, E., McTague, A., Sanchis-Juan, A., Carss, K.J., Bryant, E., Reich, A., Schneider, A.L., et al. (2019). Bi-allelic Loss-of-Function CACNA1B Mutations in Progressive Epilepsy-Dyskinesia. Am. J. Hum. Genet. *104*, 948–956.
7. Zech, M., Lam, D.D., Weber, S., Berutti, R., Poláková, K., Havránková, P., Fečíková, A., Strom, T.M., Růžička, E., Jech, R., and Winkelmann, J. (2018). A unique de novo gain-of-function variant in *CAMK4* associated with intellectual disability and hyperkinetic movement disorder. Cold Spring Harb. Mol. Case Stud. *4*, a003293.
8. Nahm, M., Lim, S.M., Kim, Y.-E., Park, J., Noh, M.-Y., Lee, S., Roh, J.E., Hwang, S.-M., Park, C.-K., Kim, Y.H., et al. (2020). *ANXA11* mutations in ALS cause dysregulation of calcium homeostasis and stress granule dynamics. Sci. Transl. Med. *12*, eaax3993.
9. Shamseldin, H.E., Alasmari, A., Salih, M.A., Samman, M.M., Mian, S.A., Alshidi, T., Ibrahim, N., Hashem, M., Faqeih, E., Al-Mohanna, F., and Alkuraya, F.S. (2017). A null mutation in MICU2 causes abnormal mitochondrial calcium homeostasis and a severe neurodevelopmental disorder. Brain *140*, 2806–2813.
10. Calì, T., Brini, M., and Carafoli, E. (2018). The PMCA pumps in genetically determined neuronal pathologies. Neurosci. Lett. *663*, 2–11.
11. Calì, T., Lopreiato, R., Shimony, J., Vineyard, M., Frizzarin, M., Zanni, G., Zanotti, G., Brini, M., Shinawi, M., and Carafoli, E. (2015). A Novel Mutation in Isoform 3 of the Plasma Membrane Ca2+ Pump Impairs Cellular Ca2+ Homeostasis in a Patient with Cerebellar Ataxia and Laminin Subunit 1α Mutations. J. Biol. Chem. *290*, 16132–16141.
12. Li, M., Ho, P.W.-L., Pang, S.Y.-Y., Tse, Z.H.-M., Kung, M.H.-W., Sham, P.-C., and Ho, S.-L. (2014). PMCA4 (ATP2B4) mutation in familial spastic paraplegia. PLoS ONE *9*, e104790.
13. Karczewski, K.J., Francioli, L.C., Tiao, G., Cummings, B.B., Alföldi, J., Wang, Q., Collins, R.L., Laricchia, K.M., Ganna, A., Birnbaum, D.P., et al. (2020). The mutational constraint spectrum quantified from variation in 141,456 humans. Nature *581*, 434–443.
14. Lindeboom, R.G.H., Supek, F., and Lehner, B. (2016). The rules and impact of nonsense-mediated mRNA decay in human cancers. Nat. Genet. *48*, 1112–1118.
15. Rentzsch, P., Schubach, M., Shendure, J., and Kircher, M. (2021). CADD-Splice-improving genome-wide variant effect

prediction using deep learning-derived splice scores. Genome Med. *13*, 31.

16. Ioannidis, N.M., Rothstein, J.H., Pejaver, V., Middha, S., McDonnell, S.K., Baheti, S., Musolf, A., Li, Q., Holzinger, E., Karyadi, D., et al. (2016). REVEL: An Ensemble Method for Predicting the Pathogenicity of Rare Missense Variants. Am. J. Hum. Genet. *99*, 877–885.
17. Mangialavori, I.C., Ferreira-Gomes, M.S., Saffioti, N.A., González-Lebrero, R.M., Rossi, R.C., and Rossi, J.P.F.C. (2013). Conformational changes produced by ATP binding to the plasma membrane calcium pump. J. Biol. Chem. *288*, 31030–31041.
18. Wiel, L., Baakman, C., Gilissen, D., Veltman, J.A., Vriend, G., and Gilissen, C. (2019). MetaDome: Pathogenicity analysis of genetic variants through aggregation of homologous human protein domains. Hum. Mutat. *40*, 1030–1038.
19. Gong, D., Chi, X., Ren, K., Huang, G., Zhou, G., Yan, N., Lei, J., and Zhou, Q. (2018). Structure of the human plasma membrane Ca^{2+}-ATPase 1 in complex with its obligatory subunit neuroplastin. Nat. Commun. *9*, 3623.
20. Kenyon, K.A., Bushong, E.A., Mauer, A.S., Strehler, E.E., Weinberg, R.J., and Burette, A.C. (2010). Cellular and subcellular localization of the neuron-specific plasma membrane calcium ATPase PMCA1a in the rat brain. J. Comp. Neurol. *518*, 3169–3183.
21. Lenz, J.C., Reusch, H.P., Albrecht, N., Schultz, G., and Schaefer, M. (2002). Ca2+-controlled competitive diacylglycerol binding of protein kinase C isoenzymes in living cells. J. Cell Biol. *159*, 291–302.
22. Salazar, M.D., Zelt, N.B., Saldivar, R., Kuntz, C.P., Chen, S., Penn, W.D., Bonneau, R., Koehler Leman, J., and Schlebach, J.P. (2020). Classification of the Molecular Defects Associated with Pathogenic Variants of the *SLC6A8* Creatine Transporter. Biochemistry *59*, 1367–1377.
23. Klein, O.D., Cotter, P.D., Schmidt, A.M., Bick, D.P., Tidyman, W.E., Albertson, D.G., Pinkel, D., and Rauen, K.A. (2005). Interstitial deletion of chromosome 12q: genotype-phenotype correlation of two patients utilizing array comparative genomic hybridization. Am. J. Med. Genet. A. *138*, 349–354.
24. James, P.A., Oei, P., Ng, D., Kannu, P., and Aftimos, S. (2005). Another case of interstitial del(12) involving the proposed cardio-facio-cutaneous candidate region. Am. J. Med. Genet. A. *136*, 12–16.
25. Schmidt, N., Kollewe, A., Constantin, C.E., Henrich, S., Ritzau-Jost, A., Bildl, W., Saalbach, A., Hallermann, S., Kulik, A., Fakler, B., and Schulte, U. (2017). Neuroplastin and Basigin Are Essential Auxiliary Subunits of Plasma Membrane Ca^{2+}-ATPases and Key Regulators of Ca^{2+} Clearance. Neuron *96*, 827–838.e9.
26. Kip, S.N., Gray, N.W., Burette, A., Canbay, A., Weinberg, R.J., and Strehler, E.E. (2006). Changes in the expression of plasma membrane calcium extrusion systems during the maturation of hippocampal neurons. Hippocampus *16*, 20–34.
27. Okunade, G.W., Miller, M.L., Pyne, G.J., Sutliff, R.L., O'Connor, K.T., Neumann, J.C., Andringa, A., Miller, D.A., Prasad, V., Doetschman, T., et al. (2004). Targeted ablation of plasma membrane Ca2+-ATPase (PMCA) 1 and 4 indicates a major housekeeping function for PMCA1 and a critical role in hyperactivated sperm motility and male fertility for PMCA4. J. Biol. Chem. *279*, 33742–33750.
28. Krebs, J. (2015). The plethora of PMCA isoforms: Alternative splicing and differential expression. Biochim. Biophys. Acta *1853*, 2018–2024.
29. Guerini, D., García-Martin, E., Gerber, A., Volbracht, C., Leist, M., Merino, C.G., and Carafoli, E. (1999). The expression of plasma membrane Ca2+ pump isoforms in cerebellar granule neurons is modulated by Ca2+. J. Biol. Chem. *274*, 1667–1676.
30. Brandt, P., Neve, R.L., Kammesheidt, A., Rhoads, R.E., and Vanaman, T.C. (1992). Analysis of the tissue-specific distribution of mRNAs encoding the plasma membrane calcium-pumping ATPases and characterization of an alternately spliced form of PMCA4 at the cDNA and genomic levels. J. Biol. Chem. *267*, 4376–4385.
31. Brini, M. (2009). Plasma membrane Ca(2+)-ATPase: from a housekeeping function to a versatile signaling role. Pflugers Arch. *457*, 657–664.

The American Journal of Human Genetics, Volume *109*

Supplemental information

De novo variants in *ATP2B1* lead to neurodevelopmental delay

Meer Jacob Rahimi, Nicole Urban, Meret Wegler, Heinrich Sticht, Michael Schaefer, Bernt Popp, Frank Gaunitz, Manuela Morleo, Vincenzo Nigro, Silvia Maitz, Grazia M.S. Mancini, Claudia Ruivenkamp, Eun-Kyung Suk, Tobias Bartolomaeus, Andreas Merkenschlager, Daniel Koboldt, Dennis Bartholomew, Alexander P.A. Stegmann, Margje Sinnema, Irma Duynisveld, Ramona Salvarinova, Simone Race, Bert B.A. de Vries, Aurélien Trimouille, Sophie Naudion, Daphna Marom, Uri Hamiel, Noa Henig, Florence Demurger, Nils Rahner, Enrika Bartels, J. Austin Hamm, Abbey M. Putnam, Richard Person, Rami Abou Jamra, and Henry Oppermann

SUPPLEMENTAL DATA

SUPPLEMENTAL NOTE: CASE REPORTS

Individual 1

Patient 1 is a 7-year-old girl who is the second child of three, born from healthy and non-consanguineous parents of European origin. The older sister and younger brother are healthy. Pregnancy and delivery were uneventful and birth parameters were within the normal range. Apgar score was 8/9. At birth dysmorphic features, hypotonia and a patent foramen ovale were noted. Karyotype and comparative genomic hybridization microarray (SurePrint G3 Human CGH Microarray 8x60K, Agilent) did not reveal any abnormalities. In the subsequent years a metabolic screening, analysis of *FMR1* gene and *ZEB2* gene (sequencing and MLPA) were normal.

At the last evaluation (age 6 years and 6 months) the patient showed weight -0.56 SD, height -1.00 SD and head circumference -1.83 SD.

Independent walking had been achieved at 21 months. The first words were reported around 30 months. Verbal communication was limited to few unintelligible words, but the girl showed good comprehension and non-verbal communication. Parents reported short attention span. No behavioral abnormalities were noted.

Medical issues comprise interatrial cardiac defect (ostium secundum) and pes planus. She experienced a febrile seizure. A cranial MRI showed a dilatation of the ventricular system

Dysmorphic features were described: coarse facial features, large and anteverted ears with dysmorphic helix, wide nasal bridge and bulbous tip. There is a supernumerary nipple. Clinodactyly of the IV toe bilaterally.

Individual 2

Patient no.2 was born after 39 weeks of pregnancy (unknown length, weight 3240 g (-0.6 SDS)) as a son of a Chinese mother and father, both parents with an unremarkable family history. He is presented with motor developmental delay (unassisted walking with 16 months) and a language development disorder became apparent (first words at 24 months).

He has autism/autism like behavior. The patient exhibits normal growth parameters but has low-set ears with overfolded helix. He was diagnosed with transposition of great vessels and according underwent surgically switch operation at birth. He lives with a residual minor pulmonalis stenosis.

Individual 3

Patient no.3 was born after 37 weeks of pregnancy (unknown length and weight) as a son (twin) of a mother and a father of European descent, both parents with an unremarkable family history. He is presented with motor developmental delay and a language development disorder became apparent.

His EEG was pathologic. A cranial MRI showed a cerebral cavernom. The patient exhibits normal growth parameters, bilateral short achilles tendons and sparse hair.

Individual 4

Patient no.4 was born after 37+3 weeks of pregnancy (length 50 cm (-0.65 SDS), weight 2860 g (-1.05 SDS)) as son of a mother of European descent and a father with Asian ancestry, both parents with an unremarkable family history. In the first year of life he presented with motor developmental delay (unassisted walking with 19 months), during the second year a language development disorder became apparent. At the age of 34 months, according to the Munich functional developmental diagnostic (MFDD) the expressive language and social skills

corresponded to the developmental age of 20 and 18 months, respectively. At that age, an autistic spectrum disorder clearly was determined.

His EEG was pathological due to epileptic discharges at the age of 2 years, first clinical seizures occurred as myoclonias and atypical absences at the age of 3 years and 2 months, a few month later a continuous spike and wave status (CSWS) was found in the sleep EEG. The epilepsy was classified as atypical childhood epilepsy with centrotemporal spikes. Clinical seizures were resistant to antiepileptic drugs: topiramate, levetiracetame, valproate and clobazam; eventually sulthiame led to clinical remission and controlled the electrical status epilepticus. Starting with the age of 6 years the body mass index slowly declined to -4.00 SDS (at the age of 17 years and 1 month length 181.4 cm and weight 41.95 kg) and he developed a distinct marfanoid habitus with arachnodactyly, S-shaped scoliosis and hypermobility of thumb.

Individual 5

This patient was born from non-consanguineous parents, at term with normal APGAR scores. Birthweight was 3,850g. The patient exhibited delayed motor milestones and delayed speech. Furthermore, he has mild ID with autistic features and some facial dysmorphia. Karyotyping at age 3 showed a <20% mosaicism for XXY (Klinefelter). MRI at age 4 showed no abnormalities. IQ tested at age 9: TIQ46, VIQ<55, PIQ<55. Adult length 194cm, armsspan 192cm, OFC 56cm.

Individual 6

The patient is a 5 years-10 months old boy, with treatment resistant epileptic encephalopathy, failure to thrive, visual cortical impairment, sensorineural hearing loss, G-tube , feeding difficulties with irritability and crying, gastroesophageal reflux, and minimally subluxated hips.

He is the 1st child to non-consanguineous parents, born after an unremarkable pregnancy, presenting with infantile spasms at 2 months of age. He has ongoing tonic seizures every 1-2 days and clusters of epileptic spasms daily currently managed with Rufinamide and CBD oil.

The patient has history of aspiration pneumonia. He is exclusively fed via G-tube, with ongoing feeding difficulties and is treated for gastroesophageal reflux disease. He has managed with minimally subluxed hips bilaterally.

Clinical evaluation at age of 2 years revealed mild dysmorphology including: low anterior hairline and a ridge at the line of the coronal suture, flattened occiput, relatively thin, arched eyebrows and long eyelashes, deep set eyes and a prominent forehead, broad nasal root and a bulbous nasal tip, excess nuchal skin and no neck widening. He had fleshy palms, deep palmar creases and subcutaneous adipose creases on the medial aspect of his calves, and above his popliteal fossae bilaterally.

Developmentally the patient shows severe delay and requires full care. In terms of motor skills he is able to roll. He has cortical visual impairment, nystagmus and variable alternating exotropia with a slight optic nerve pallor. He is wearing hearing aids in view of bilateral sensory neural hearing loss.

Biochemical investigations in blood, urine, and CSF were unremarkable. Chromosomal microarray was normal male. Clinical trio exome sequencing with mtDNA sequencing identified *de novo* heterozygous variant c.2365C>T, p.(Arg789Cys) in *ATP2B1*.

Individual 7

This 17 years old girl was born after a normal pregnancy at term with a birth weight of 3500 gram. She developed seizures at the age of 4 months and, subsequently regressed. She was

diagnosed with West syndrome at the age of 6 months. She responded well to Sabril at 10 months and remained free of seizures. She started walking independently and speaking first words at 3 years of age. MRI of the brain revealed no abnormalities and also metabolic studies were normal. Her level was ascertained and she had an IQ of 58. She developed behavior problems with obsessive aspects.

She had a normal growth with height of 175 cm (75th centile) and head circumference of 55.5 cm (25th centile). She did not have any facial dysmorphism.

Whole exome sequencing revealed a *de novo* missense variant in *ATP2B1*, c.2470G>A, p.(Glu824Lys).

Individual 8

Patient no.8 was born after 39 weeks of pregnancy (length 47 cm, weight 3100 g (-0.6 SDS)) as a daughter of a Moroccan mother and father, both parents with an unremarkable family history. She has an older brother in good health. At birth, Apgar score was 6/10, and she needed to be hospitalized for respiratory distress with no known etiology.

During the first year of life, she had been hospitalized for dyspnea with stridor, vomiting, and feeding difficulties.

She is presented with motor developmental delay (sitting with 12 months) and a language development disorder became apparent (first words at 26 months). The patient exhibits normal growth parameters. Clinical examination shows brachycephaly, very low hairline on the forehead, bilateral epicanthus, very long eyelashes, bulbous nasal tip, hat-shaped mouth, ogival palate, and hirsutism. She has low implanted thumbs, deep palmar folds and clinodactyly of the 5th fingers. She also has hepatomegaly with cholestasis. In addition to the *ATP2B1* variant c.2570A>G, p.(Gln857Arg), WES analysis found an additional *WDR83OS*

homozygous variant, possibly involved in the hepatic symptoms: NM_016145.3:c.255-4_260del, p.?.

Individual 9

Patient no.9 is a 51 years old male manifesting a simplex case of early childhood nonprogressive global developmental delay. Later on, he was diagnosed with mild syndromic intellectual disability (IQ 73), learning and behavioral difficulties and high function autism spectrum disorder. He attended special education and is now leading a nearly total independent life, living on his own and being employed. Physical findings include a marfanoid habitus, tall stature 183 cm (80th percentile), head circumference 57.5 cm (75th percentile), arachnodactyly (total hand length and middle finger length 22cm & 13cm both > 97th percentile), low folded soft earlobes, high-arched palate, pectus carinatum, scoliosis, mild DIP and PIP camptodactyly and club foot. Hypertelorism was ruled out. Recent echocardiography revealed mild aortic root dilation but an otherwise structurally normal heart. He has no other congenital anomalies. Hearing and eye examination are normal.

Prior (2014-2016) genetic studies (CMA, Fragile X, maternal X inactivation analysis and singleton clinical exome) were all unremarkable.

Individual 10

Patient no.10 was born after 40 weeks of pregnancy (length 47 cm, weight 2650 g (-2.2 SDS)) as a son of a mother and father of European descent, both parents with an unremarkable family history. He is presented with motor developmental delay and a language development disorder became apparent.

He shows signs of hyperactivity. The patient exhibits normal growth parameters but has some craniofacial abnormalities like sparse eyebrows or palpebral edema.

Individual 11

Patient no.11 was born after 40 weeks of pregnancy (length 52 cm (+0.1 SDS), weight 3450 g (0 SDS)) as a daughter of a mother and father of European descent, both parents are without an education/qualification. The father especially was a late talker (with 7 years). She is presented with a language development disorder became apparent. A SONR 2 1/2-7 non-verbal intelligence test at the age of 4.4 years displayed a cognitive performance as at 2.2 years of age. The patient exhibits a short stature and has no other abnormalities.

Individual 12

Patient no.12 is a 5 year old son of a Chinese mother and father, both parents with an unremarkable family history. He is presented with motor developmental delay (unassisted walking with 21 months) and is nonambulatory and nonverbal.

He experienced infantile spasms. A cranial MRI showed a small area of gliosis or encephalomalacia of the left caudate nucleus. Furthermore, he has autism/autism like behavior and lives with anxiety, sleeping and mood problems. The patient exhibits normal growth parameters but has esotropia and plagiocepahly. He has some congenital malformations like PFO, cryptorchidism, hypospadias, pectus excavatum and sacral dimple.

Individual 16 (excluded from the clinical description)

Individual 16 is a 5-year-old male (born Aug 2016) of European ancestry. He came to medical attention during the prenatal period when an ultrasound noted bilateral CL/P and significant

oligohydramnios. He was born at term but admitted to the NICU due to feeding issues and apneic spells. He was referred to clinical genetics at 17 months of age for evaluation of multiple issues including failure to thrive, hypotonia, developmental delay, dysmorphic features, and a single seizure (at age 4 months). He had a striking macrocephaly (>99th percentile) and CL/P (surgically repaired), both of which were present in his mother. He was also noted for triangular facies, slight ptosis, inferior inner epicanthal folds, and downslanting palpebral fissures. His most recent brain MRI (2019) was normal, and his seizures (generalized tonic-clonic seizures of unknown etiology) have been under control with Keppra. Though noted for poor intestinal motility, his appetite has improved. He has ongoing developmental delays and receives physical, occupational, and speech therapies. After a non-diagnostic clinical WES (2018), he was referred for further genomic studies under an IRB-approved research study at Nationwide Children's Hospital. Trio whole-genome sequencing revealed a *de novo* variant in *ATP2B1*, NM_001682.3:c.1793T>C, p.(Ile598Thr), which was confirmed by Sanger sequencing. Structural protein modeling suggested that this variant not critically affect ATP2B1 structure, as Ile598 is rather solvent exposed. Furthermore, the membrane localization (0.57±0.11; wild-type:0.6±0.07; $p>0.05$) and the tau-vale (12.67±1.33; wild-type:12.66±1.41; $p>0.05$) of p.Ile598Thr was indistinguishable from the wild-type. Thus, as the relevance of this variant is uncertain, we excluded this individual from the phenotypic analysis.

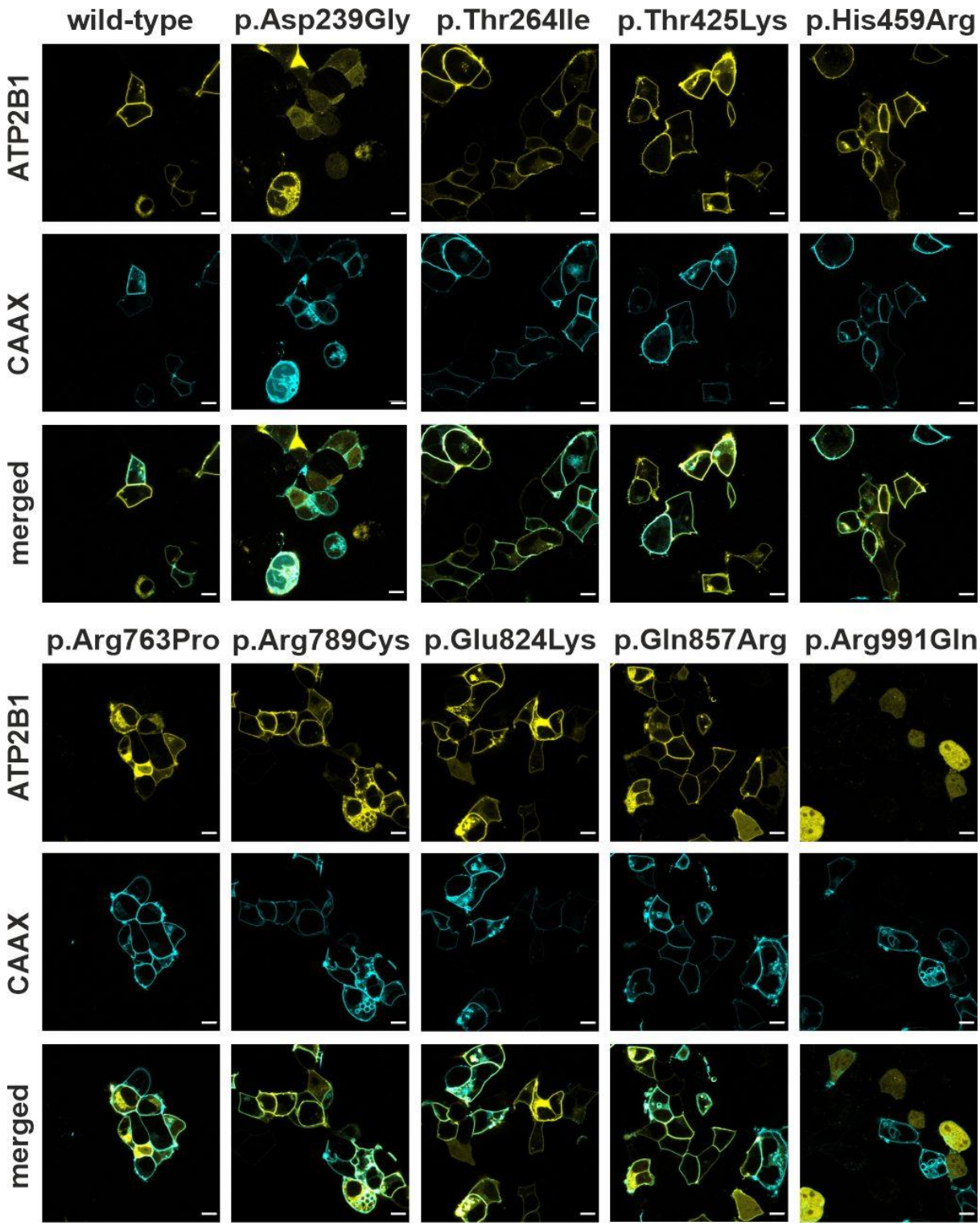

Figure S1: Subcellular localization of transiently overexpressed *ATP2B1* variants. (A) Representative confocal laser scanning microscopy images of transfected HEK293 cells expressing YFP-fused ATP2B1 and a CAAX-box-modified cyan fluorescent protein. Scale bars: 10 µm.

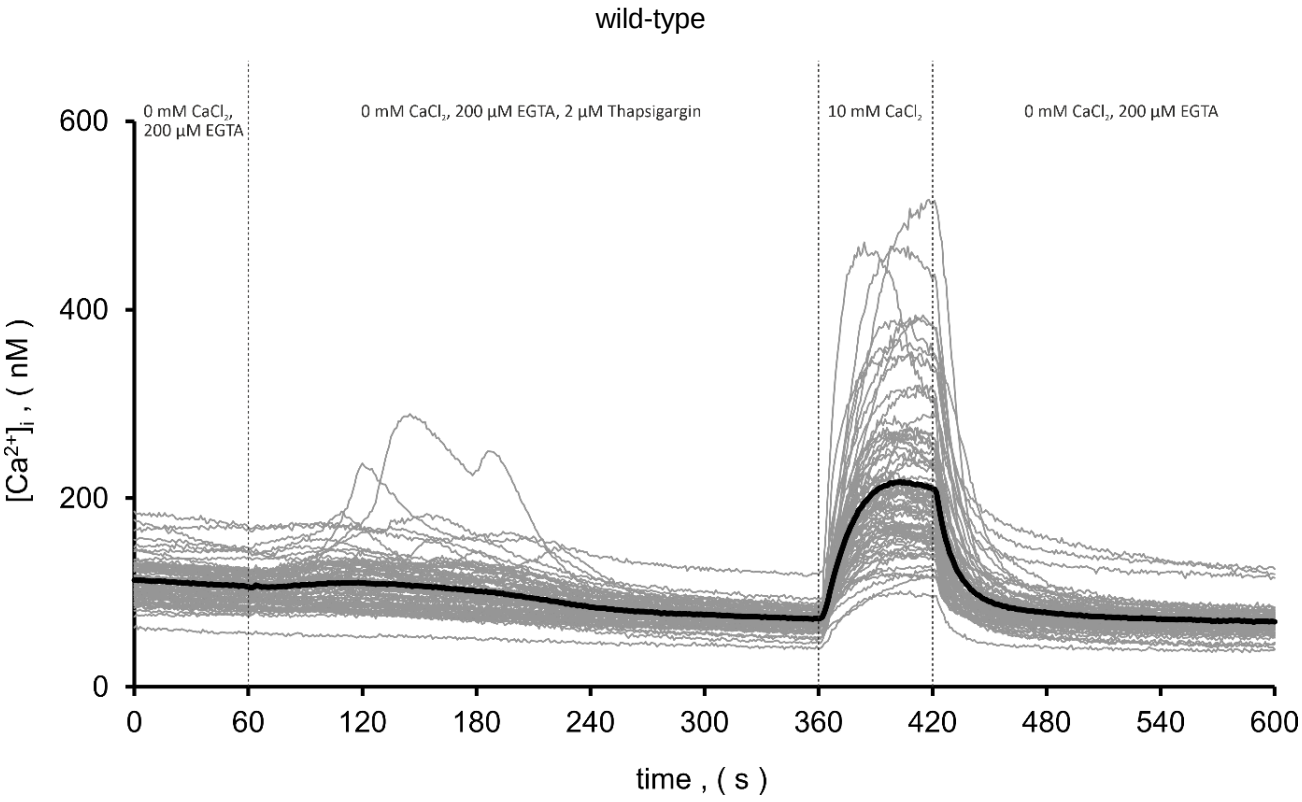

Figure S2: Detailed fluorometric $[Ca^{2+}]_i$ analysis (for details see methods) of fura-2-loaded HEK293 cells overexpressing ATP2B1 wild-type. Shown are representative recordings of $[Ca^{2+}]_i$ in 75 single cells (grey lines) and averaged signal (black line) during perfusion with various buffer conditions as indicated. Time-dependent $[Ca^{2+}]_i$ decline in Figure 4 was calculated from interval 420 s to 540 s.

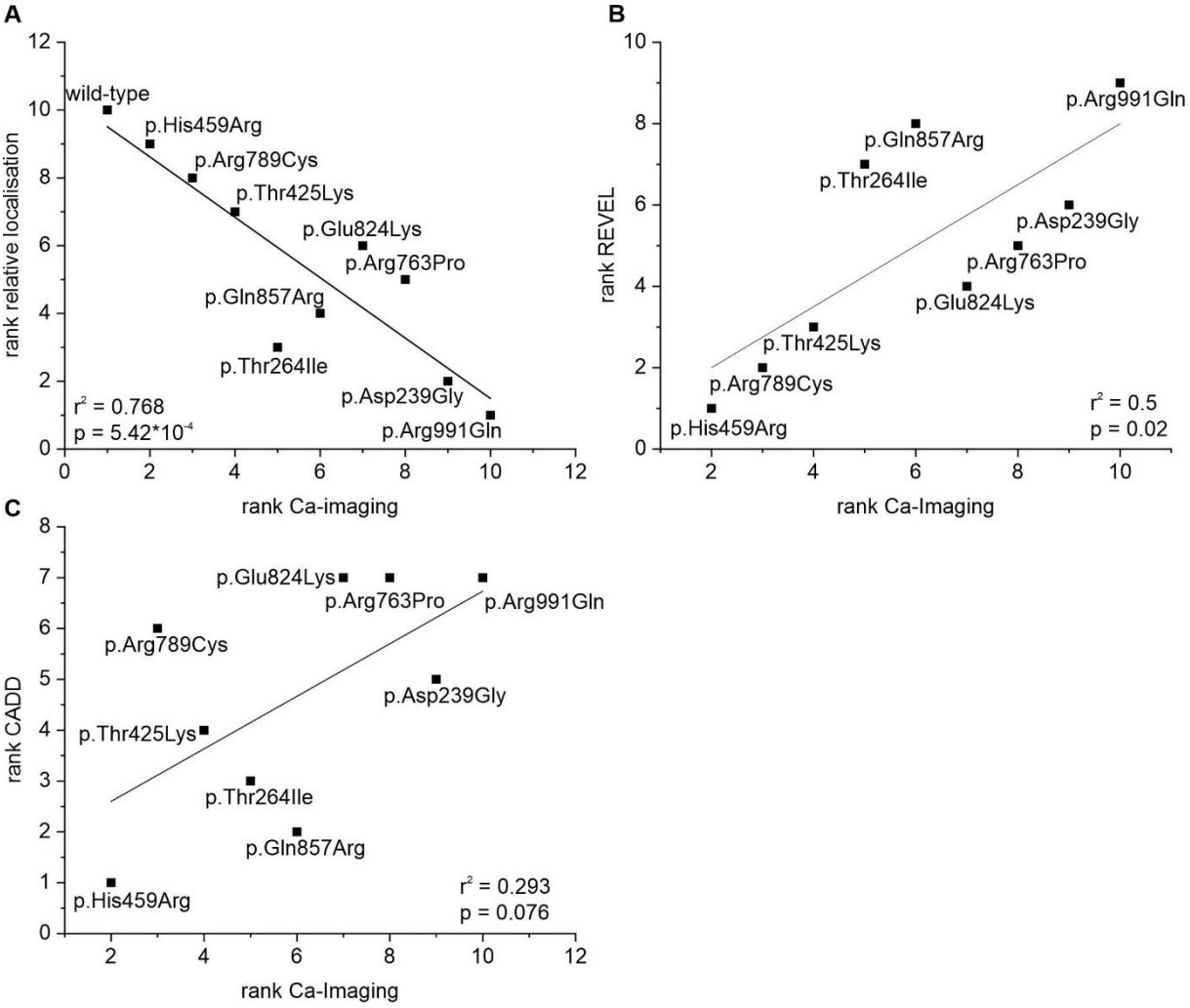

Figure S3: Correlation between tau-value, cellular localization and REVEL and CADD. (A) Correlation between $[Ca^{2+}]_i$ imaging and membrane co-localization of the *ATP2B1* variants (for details see methods) Each variant was ranked in both experiments dependent on tau-value and PCC-value. The lowest tau-value ranks at number one and the lowest PCC-value ranks as number one in relative localization. The x-axis represents the ranking of tau-value, the y-axis the ranking in relative localization. Correlation (B) between tau-value and REVEL score and (C) between tau-value and CADD score of each variant. The lowest tau-value ranks at number one again and the lowest REVEL and CADD score ranks as number one, respectively.

SUPPLEMENTAL METHODS

PATIENT STUDY

Collaborative efforts via online platforms like GeneMatcher[1] and DECIPHER[2] from different centers in Germany, the Netherlands, New Zealand, Canada, Israel, Italy, USA and France resulted into the cohort of this study. Physicians and geneticists contributed detailed clinical and genetic information, via routine clinical examination or in a research setting. In total, around 95,000 trio-exomes, exomes or genomes were analyzed in a clinical or research setting to identify 26 independent individuals with a *ATP2B1* variant. Thirteen individuals were deemed relevant and included in this study. All analyses were performed in concordance with the provisions of the German Gene Diagnostic Act (Gendiagnostikgesetz) and the General Data Protection Act (Bundesdatenschutzgesetz) for the German patients. Written informed consents of all examined individuals or their legal representatives were obtained for genetic testing and publication after advice and information about their risks and benefit. We have also collected three additional individuals that have a *de novo ATP2B1* variant, which were identified in the Deciphering Developmental Disorders Study[3]. As these variants were identified by trio-exome sequencing without further interpretation, a causal relationship of *de novo* variants in *ATP2B1* and a disorder has not been demonstrated, yet. We have not included these individuals into the clinical and variant description, as we could not acquire a detailed phenotypic description (see Figure1 and Table S1).

Sequencing, Identification and Evaluation of variants

For all cases, exome or genome sequencing were performed by using standard commercial products within a diagnostic setting. All cases were evaluated in a clinical setting and no

reportable variants were identified. After families consented for research, evaluation of the data was continued in a scientific setting. The variants were prioritized based on minor allele frequency, inheritance mode, potential predicted pathogenicity (based on several *in silico* predictions), attributes of the genes, including functional plausibility, tolerance for variants (i.e. LOEUF value and Z-Score), as well as further aspects including available animal models, interaction partners, tissue expression (the Genotype-Tissue Expression (GTEx)) and plausibility of the symptoms in regard to the function of the gene. This analysis yielded a variant in *ATP2B1* as the most promising candidate.

ATP2B1 expression plasmids

Full-length human *ATP2B1* open reading frame (ORF; GeneBank: NM_001001323.2) cDNA was obtained by PCR from healthy human brain cDNA (normal brain tissue, parietal lobe, lot. 811001, BioCat GmbH, Heidelberg, Germany) by using specific primers (Table S2) and the PfuUltra II Hotstart PCR Master Mix (Agilent Technologies, Waldbronn, Germany) according to the manufacturer's recommendation. Fragments of the *ATP2B1* ORF were amplified by PCR (Table S2) from *ATP2B1* cDNA and subcloned with the Zero Blunt TOPO PCR Cloning Kit (ThermoFisher Scientific, Darmstadt, Germany). The *ATP2B1* open-reading frame fragments were assembled by using the Golden Gate Assembly Kit (BsmBI-v2; New England Biolabs GmbH, Frankfurt am Main, Germany) according to the manufacturer's recommendation. Afterwards, the *ATP2B1* open-reading frame without a stop codon was in-frame ligated into a pcDNA3 expression vector containing the ORF of enhanced yellow fluorescent protein (YFP) by using *EcoR*I and *Xba*I restriction enzymes. Mutagenesis was performed by using the QuikChange II XL site-directed mutagenesis kit (Agilent Technologies) according to the manufacturer's recommendation. All sequences were verified by Sanger sequencing.

Cell Culture and Transfection

Transfection was performed as described previously[4]. Briefly, HEK293 cells were cultured in Eagle's Minimum Essential Medium (Sigma, Munich, Germany), supplemented with 10% fetal calf serum, 2 mM L-glutamine, 100 $U \cdot mL^{-1}$ penicillin, 0.1 $mg \cdot mL^{-1}$ streptomycin (all from Thermo Fisher Scientific) and incubated at 37°C and 5% CO_2 in humidified air in an incubator. For transfection, HEK293 cells were seeded on 25 mm glass coverslips and transfected with 4 µL JetPEI (Polyplus, Illkrich, France) and 2 µg of DNA encoding wild-type or mutated variants of ATP2B1-YFP.

Microfluorometric $[Ca^{2+}]_i$ imaging analysis

Fluorometric $[Ca^{2+}]_i$ assays in HEK293 cell lines were performed as described previously[5]. Briefly, HEK293 cells were transfected and loaded with 4 µM fura-2/AM (AAT Bioquest, Sunnyvale, California, USA) in HBS (132 mM NaCl, 6 mM KCl, 1mM $MgCl_2$, 1mM $CaCl_2$, 5.5 mM D-glucose and 10 mM HEPES, 0.1% BSA; pH 7.4) for 30 min at 37°C.

$[Ca^{2+}]_i$ measurements were performed on an inverted epifluorescence microscope with a Fluar 10×/0.5 objective (Carl Zeiss, Jena, Germany) and calibrated as described before[4, 5]. The measurements spanned 600 seconds with images taken in an interval of one second. HEK293 cells on coverslips were mounted in a bath chamber and superfused with HBS containing 200 µM EGTA. After internal Ca^{2+} store depletion with HBS containing 2 µM thapsigargin, the cells were perfused with HBS containing 10mM $CaCl_2$, followed by nominally Ca^{2+}-free HBS with 200 µM EGTA again. The time constant tau of declining $[Ca^{2+}]_i$ was calculated in GraphPad Prim 9 (Graphpad Software, Inc.; Version: 9.2.0 64-bit) by a curve fit with the function: $y=(y_0$ -

Plateau) * exp (-K * x) + Plateau, based on $[Ca^{2+}]_i$ measurements after the final addition of EGTA. The Plateau corresponds to the basal $[Ca^{2+}]_i$.

Fluorescence microscopy

HEK293 cells were transfected with the corresponding ATP2B1-YFP plasmid and with an expression plasmid that encodes a membrane-targeted cyan fluorescent protein (CAAX-box motif fused for lipid modification; CAAX). Afterwards fluorescence images were taken by using a LSM 510-META confocal laser scanning microscope (Zeiss, Jena, Germany). To determine the relative membrane localization, we analyzed the co-localization of expressed ATP2B1 and CAAX by using the EzColocalization plugin according to Stauffer *et al.* in ImageJ (version: 1.8.0_172)[6, 7]. Results are shown as Pearson correlations coefficient (PCC), which measures the correlation between pixel values for two reporter channels. A value of 0 indicates non-colocalization and a value of 1 complete co-localization.

Structural Modeling

The structural analysis of the variants was based in the cryo-EM structure of *ATP2B1* in complex with neuroplastin (PDB: 6A69[8]). Variants were modelled with Swiss-Model[9], and RasMol[10] was used for structure analysis and visualization.

Protein tolerance landscape

The tolerance landscape, as obtained by MetaDome[11], was obtained from the public available web server (https://stuart.radboudumc.nl/metadome). The algorithm maps population

variation from the Exome Aggregation Consortium (ExAC) and pathogenic variants from the Human Gene Mutation Database (HGMD) and ClinVar onto Pfam protein domains. Based on domain homology, a genetic intolerance is calculated on amino acid resolution for human protein domains.

Statistical analysis

Statistical analysis was carried out using GraphPad Prism 9 and OriginPro 2019 (version: 9.6.0.172, OriginLab, Northampton, United States). We used a one-way ANOVA with the Games-Howel post hoc test for multiple comparisons. If not stated otherwise, data is presented as mean ± standard deviation. A p-value < 0.05 was presumed to be statistically significant.

References

1. Sobreira, N., Schiettecatte, F., Valle, D., and Hamosh, A. (2015). GeneMatcher: a matching tool for connecting investigators with an interest in the same gene. Human mutation *36,* 928–930.

2. Firth, H.V., Richards, S.M., Bevan, A.P., Clayton, S., Corpas, M., Rajan, D., van Vooren, S., Moreau, Y., Pettett, R.M., and Carter, N.P. (2009). DECIPHER: Database of Chromosomal Imbalance and Phenotype in Humans Using Ensembl Resources. American journal of human genetics *84,* 524–533.

3. Kaplanis, J., Samocha, K.E., Wiel, L., Zhang, Z., Arvai, K.J., Eberhardt, R.Y., Gallone, G., Lelieveld, S.H., Martin, H.C., and McRae, J.F., et al. (2020). Evidence for 28 genetic disorders discovered by combining healthcare and research data. Nature *586,* 757–762.

4. Urban, N., Neuser, S., Hentschel, A., Köhling, S., Rademann, J., and Schaefer, M. (2017). Pharmacological inhibition of focal segmental glomerulosclerosis-related, gain of function mutants of TRPC6 channels by semi-synthetic derivatives of larixol. British journal of pharmacology *174,* 4099–4122.

5. Lenz, J.C., Reusch, H.P., Albrecht, N., Schultz, G., and Schaefer, M. (2002). Ca2+-controlled competitive diacylglycerol binding of protein kinase C isoenzymes in living cells. The Journal of cell biology *159,* 291–302.

6. Stauffer, W., Sheng, H., and Lim, H.N. (2018). EzColocalization: An ImageJ plugin for visualizing and measuring colocalization in cells and organisms. Scientific reports *8,* 15764.

7. Schneider, C.A., Rasband, W.S., and Eliceiri, K.W. (2012). NIH Image to ImageJ: 25 years of image analysis. Nature methods *9,* 671–675.

8. Gong, D., Chi, X., Ren, K., Huang, G., Zhou, G., Yan, N., Lei, J., and Zhou, Q. (2018). Structure of the human plasma membrane Ca2+-ATPase 1 in complex with its obligatory subunit neuroplastin. Nature communications *9,* 3623.

9. Guex, N., and Peitsch, M.C. (1997). SWISS-MODEL and the Swiss-PdbViewer: an environment for comparative protein modeling. Electrophoresis *18,* 2714–2723.

10. Sayle, R.A., and Milner-White, E.J. (1995). RASMOL: biomolecular graphics for all. Trends in biochemical sciences *20,* 374.

11. Wiel, L., Baakman, C., Gilissen, D., Veltman, J.A., Vriend, G., and Gilissen, C. (2019). MetaDome: Pathogenicity analysis of genetic variants through aggregation of homologous human protein domains. Human mutation *40,* 1030–1038.